Photon-gated foldaxane assembly/disassembly

Chenhao Yao, Bappaditya Gole, Anh Thy Bui, Brice Kauffmann, Ivan Huc, Nathan D Mcclenaghan, Yann Ferrand

Photon-gated Foldaxane Assembly/Disassembly

Chenhao Yao,[a] Bappaditya Gole,[ab] Anh Thy Bui ,[c] Brice Kauffmann,[d] Ivan Huc,[e] Nathan D. McClenaghan,[*c] and Yann Ferrand[*a]

Integrating multiple anthracene motifs into aromatic oligoamide sequences gives rise to photoactive foldamers that can sequester a molecular thread forming helix-on-axle assemblies. Photoirradiation is shown to distort the helical host and drive dissociation of the supramolecular assembly and thread liberation as signalled by a photonic output, while thermal reversion regenerates the assembly.

Aromatic oligoamide foldamers have emerged as a versatile class of functional molecules, which adopt robust folded conformations whose properties can be finely tuned based on the chosen sequence of monomers.[1] Judicious design of such foldamers has been shown to offer cavities for strong and selective binding of a range of guest molecules[2] and, more recently, photoactivity has been introduced both in terms of emission and photoreaction.[3] Foldaxanes,[4,5] supramolecular architectures comprising aromatic helices on a linear molecular axle, represent a recent addition to the field of interpenetrating molecules.[6] Reported examples focus on their formation evoking specific complementary hydrogen-bonding motifs and on-axle helix translation dynamics[7] and assembly rates.[7,8] Herein, we consider a supramolecular two-component system, where light can be used to both control the assembly and act as a signalling mechanism of association (or dissociation) through a fluorescence output. This functioning is reminiscent of a 2-stroke molecular piston,[9] based on a unique foldaxane architecture, combining both light- and thermally-driven steps.

In the current design, as shown schematically in Fig. 1, an unbound T-shaped guest is anticipated to give a specific optical response, a characteristic exciplex emission resulting from an intramolecular interaction between amine (green) and fluorophore (blue). Binding and interpenetration within a helix-sheet-helix foldamer[3,10] would result in the guest adopting a more extended conformation, spatially decoupling amine and fluorophore and modulating the observed emission. While a light output would signal the state of the system, a light input could also drive guest photoexpulsion based on steric demands mediated by a reversible [4π + 4π] photocycloaddition reaction. The structural formulas of molecules developed and studied herein (Fig. 2), include a symmetrical host sequence **1**, integrating diazaanthracene units in a bent three stranded sheet A^F-T-A^H-T-A^F, flanked with two helical segments comprising a tetrameric amide sequence of 7-amino-8-fluoro-2-quinolinecarboxylic acid (Q^F_4) providing a cylindrical cavity which is large enough to accommodate a linear alkyl chain. Terminal polar pinchers (P_3) comprising pyridine dicarboxamides are capable of binding to each carbonyl of the guest. Sequence **1a** corresponds to a photoproduct implying a photocycloisomerisation of two parallel anthracene-like moieties, while **2** is a symmetrical dye-free thread.

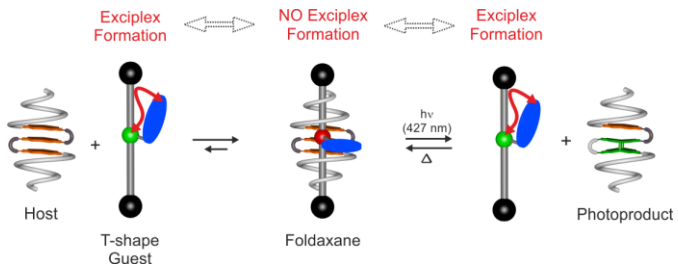

Fig. 1. Schematic representation of equilibrium of the self-assembly of helix-sheet-helix host and T-shape guest to form the foldaxane (left) and reactions involved in the photoswitchable process (right). The photoreaction and thermal reversion can control the release and uptake of the guest, respectively. The free T-shape rod can form an intramolecular exciplex, interacting groups denoted by a red arrow, which will be disrupted in the foldaxane.

Helix-sheet-helix **1** was obtained via a convergent synthetic strategy, as detailed in the ESI (Schemes S1-S3).† Briefly, the conical $P_3Q^F_4$ segment was first prepared and transiently functionalised with a labile dimethoxybenzyl (DMB) group able to prevent the aggregation of the aromatic strands during the synthesis.[11] The amino group of the helical segment was connected at each end of the A^F-T-A^H-T-A^F bent sheet dicacid and after purification the two DMB groups were removed under acidic conditions.

Evidence for host-guest association in solution was provided by ^{1}H NMR spectroscopy in CD_2Cl_2 (Fig. 3a-d). Mixing **1** with a linear **2** or T-shaped **3a** thread led to significant deshielding of N-H proton resonances, indicative of hydrogen bonding between the carbamate groups of the thread and the amide groups of the host located in the terminal P_3 polar pinchers, as represented in Fig. 2e. The NMR spectrum of complex **1**⊃**3** was globally similar to that of aforementioned **1**⊃**2**, but given the non-symmetrical

nature of the thread and hence non-equivalence of these functional groups, the number of resonances was doubled. Equally, shifting of aromatic proton signals associated with the foldamer was observed upon binding. In particular, shifts of CH aromatic protons from both the T turn unit (H_{ext}) and protons on the central ring of the A^H unit (H9 and H10) were diagnostic of strong interaction and modification of the internal cavity environment.

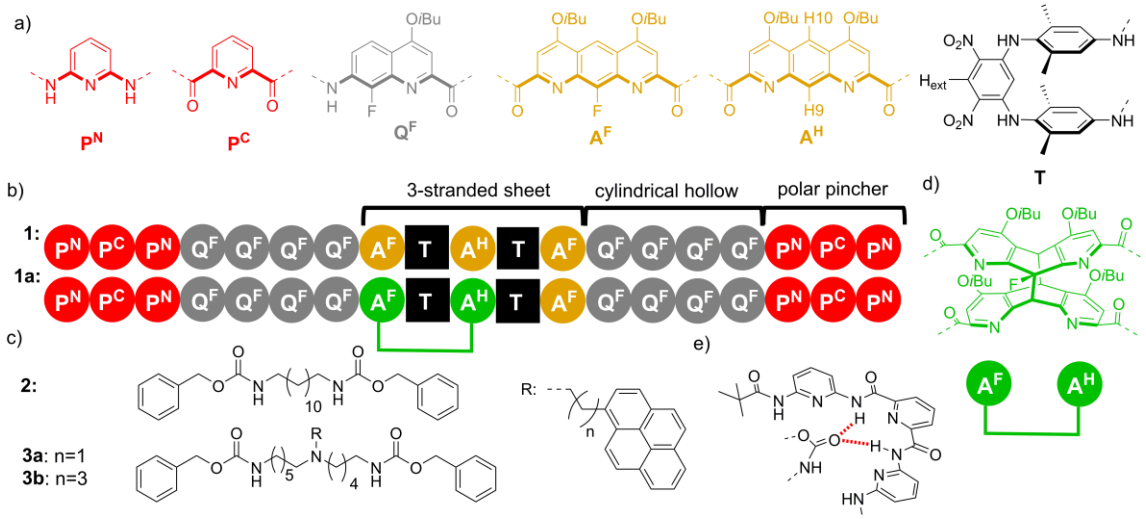

Fig. 2. Representation of: a) Colour formula and letter of the diamine, diacid and amino acid monomers. b) Oligoamide sequences of **1** and **1a**. Note that **1a** is the photoproduct arising from **1**. c) Formula of linear guest **2** and T shape guest **3**. d) A parallel diazaanthracene photoproduct in the aromatic sheet. e) Binding mode of a carbamate in a polar pincher. The binding is stabilised by intermolecular hydrogen bonds (dotted red lines).

Titrations of host **1** with guest **2** in CD_2Cl_2 gave an affinity constant (K_a) of 6.47 x 10^4 L.mol^{-1} and a 1:1 stoichiometry, while a slightly lower value of 2.63 x 10^4 L.mol^{-1} was obtained for **1**⊃**3a** (Figs. S1-S3). A single crystal X-ray analysis of **1**⊃**3a** (Fig. 3e-g, Fig. S4) gave conclusive evidence of the interpenetrating nature of the foldaxane assembly and indications on the key binding features. Short C=O···N-H contact distances of 2.13 Å and 2.06 Å designate the carbamate interaction with the polar pinchers, while the pendant pyrene sub-unit occupied the void in the helical backbone. Additionally, in **1**⊃**3a** the π-system of the appended pyrene adopted a face-to-face orientation with a proximal electron-poor dinitroaromatic of one of the turn units T, which is consistent with the shielding of the H_{ext} proton resonance (Fig. 3c vs. Fig. 3b, triangles).

Concerning the optical properties of **3a** and **3b**, the parent 1-alkylpyrene chromophore typically gives intense structured absorption and fluorescence in the near UV spectral region.[12] However, incorporating such a fluorophore into the thread via an alkyl tether in close proximity to a tertiary amine group may be anticipated to modify the observed excited-state properties. Indeed, thermodynamically and kinetically-favourable photoinduced electron transfer may occur from amines to excited fused aromatics across simple methylene spacers, as popularised by de Silva and coworkers,[13] whereas when longer linkers are incorporated different responses may be observed. Notably, De Schryver and coworkers showed that an N-pyrene excited-state complex / exciplex was observed in specific cases in solvents of low-to-medium polarity, and optimal with 2 or 3 methylene group spacers.[14] Disruption of the exciplex on foldaxane formation, as well as modulation of electronic energy transfer, was targeted as the optical signalling mechanism in the current work and as such, **3a** and **3b** integrating a 2 and 4-methylene spacer, respectively, between amine and pyrene were synthesised. In homogeneous and dilute chloroform (or dichloromethane) solution, structured fluorescence as well as a dominant broad lower energy emission band was observed in the case of **3a** in toluene and dichloromethane solvents (ϕ_F = 0.26) but is greatly diminished in intensity in highly polar DMSO (Fig. S5). Further, varying concentration had minimal effect on the relative intensities of each emission band in **3a** consistent with the emission being intramolecular in origin, ruling out excimer formation at these concentrations. In contrast, in the case of **3b** (ϕ_F = 0.05) at similar (sub-mM) concentration non-structured emission was minimal (Fig. S6), while at concentrations higher than 1 mM the excimer emission became increasingly intense.

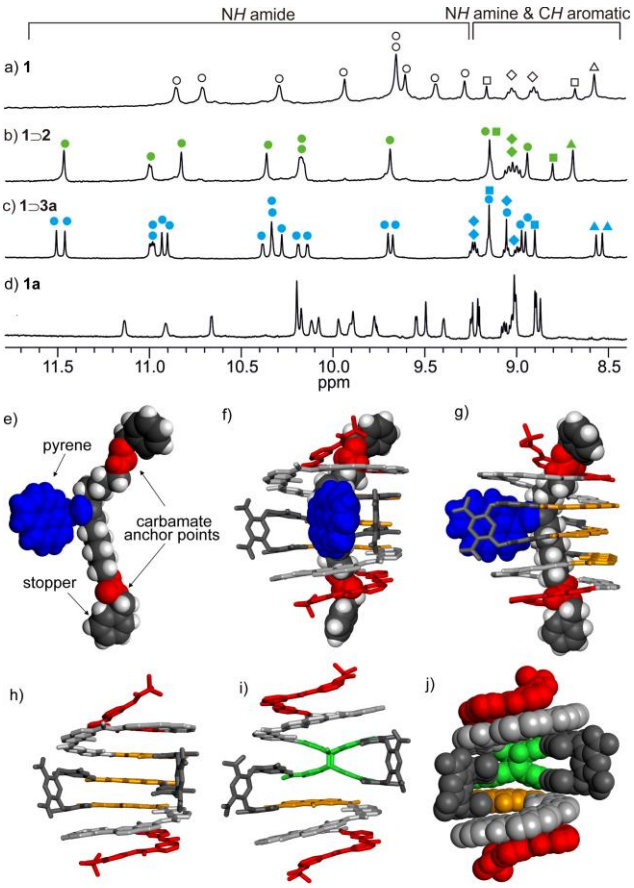

Fig. 3. Part of the ^{1}H NMR spectra (CD_2Cl_2, 400 MHz) of : a) 0.5 mM **1** in absence of guest; b) 0.5 mM **1** in the presence of **2** (5 equiv); c) 0.5 mM **1** in the presence of **3a** (5 equiv); d) **1a**. NH amide protons, NH amine protons, CH aromatic protons from A^H unit (H9 and H10) and H_{ext} are marked as circles (O), diamonds (◊), squares (□) and triangles (Δ), respectively. Signals of the free symmetrical host, symmetrical foldaxane **1⊃2** and unsymmetrical foldaxane **1⊃3a** are marked and filled with empty, green, and blue circles, respectively. Structures in the solid state analysed by X-ray crystallography of: e) T-shape guest in the crystal packing; and f) Front view and g) Side view of foldaxane **1⊃3a**. The guest is shown as a CPK representation and the host is shown as a stick representation. h) Host **1** as it exists in the structure of **1⊃3a**. Front view of the energy-minimised molecular models (using Merck Molecular Force Field static, MMFFs) of **1a** in stick representation (i) and CPK representation (j). The carbamate and pyrene in the T-shape guest are marked in red and blue, respectively. The monomers in the host are colour coded as in Fig. 2. Side chains (O^tBu groups) of host and included solvent molecules have been removed for clarity.

Foldamer host **1** fluorescence was typically broad, short-lived and very weak (ϕ_F = ca. 0.001, Figs. S7, S8), anthracene quenching being attributed to downhill electronic energy transfer. Diazaanthracence (A^F-A^H-A^F) sub-units were integrated In the host capsule in a parallel orientation at distances (<4 Å) compatible with a A^F-A^H cycloisomerisation reaction, as shown in the single crystal X-ray structure (Fig. 3h). Diazaanthracene units have a high propensity to undergo homo- and hetero-photocyclisation reactions, often exhibiting higher reaction quantum yields and resistance to secondary photoreactions than parent anthracene.[3,15] Photoirradiation of **1** in argon-bubbled halogenated solvents cleanly gave **1a** as denoted by shifting bridgehead proton resonances accompanying the C sp^2-to-sp^3 conversion. Notably the appearance of ^{1}H resonances between 5 - 5.5 ppm further

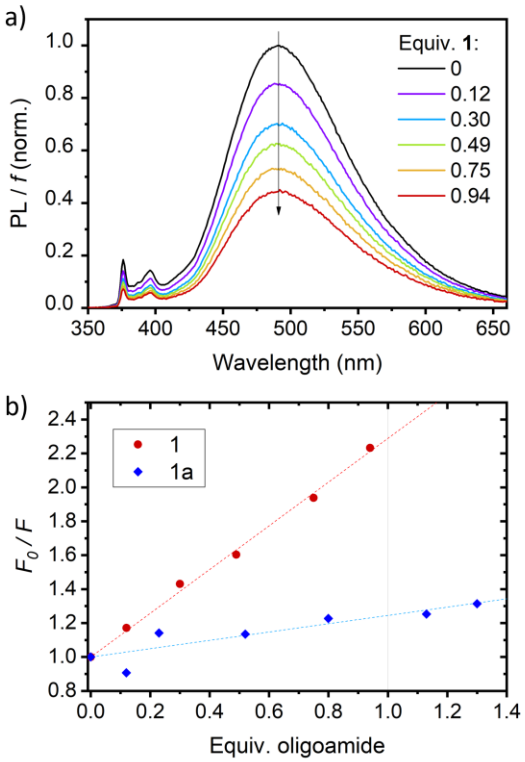

Fig 4. Quenching effect of host **1** on the fluorescence of a 0.5 mM solution of **3a** in CH_2Cl_2 (λ_{exc} = 335 nm) in the presence of Et_3N (1.5 mM). a) Fluorescence emission spectra of **3a** with increasing number of equivalents of **1** at constant volume, corrected by f, the amount of light absorbed by **3a** (see ESI). b) Quenching plots obtained upon addition of **1** or **1a** to **3a**. *F* is the integral of the corrected fluorescence, and F_0 is the value measured in the absence of foldamer (lines are guides for the eye).

exhibiting coupling with the fluorine, while the ^{19}F resonance at 160 ppm is characteristic of a photocyclised A^F-A^H pair of anthracenes (see Fig. S11, S15).[3b] The model of the photoproduct was obtained via molecular mechanics (Fig. 3i), revealing the formation of **1a** and 2 C-C bonds between the central anthracene A^F and one of the A^H central cycles. With photoproduct **1a** in hand, binding studies using either **1** or **1a** with threads were performed (Fig. S9). While titrating guest **3a** with helix **1** in CH_2Cl_2 led to a marked decrease of the exciplex emission band ascribed to complexation (Fig. 4a; ϕ_F dropping from 0.26 to 0.06), fluorescence emission showed virtually no capsule-induced quenching when adding **1a** (Fig. 4b), consistent with the absence of guest binding, further corroborated by NMR (Fig. S11-13). Consequently, photoswitching the foldaxane assembly would result in a lessened guest affinity and light-driven guest release. ^1H NMR spectroscopy showed that in **1⊃3a**, the cycloisomerised photoproduct was formed more slowly upon irradiation than in the free host **1** (Fig. 5a), as revealed by quantum yields obtained from photoconversion kinetics fits (ϕ_{PC} = 8.3×10^{-4} and 2.8×10^{-4}, for **1** and **1⊃3a** respectively; Fig S10). The thermal reversibility of the reaction was further demonstrated, with the shifted proton resonances being restored to their original position on heating (Fig. S11,12). Tests of reversible foldaxane assembly and disassembly cycles were carried out, and two full ejection-uptake cycles were successfully performed and monitored by NMR (Fig. S13) and fluorescence switching (Fig. 5b), albeit with a small amount of unidentified secondary photoproduct.

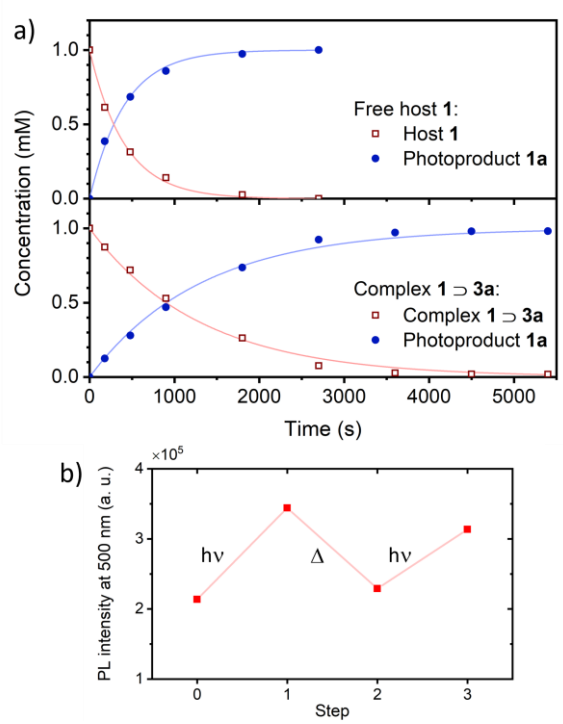

Fig. 5. Release and uptake of guest **3a**. a) Time evolution of the concentrations of the different species upon irradiation at 427 nm, as determined by ^{1}H NMR (CD_2Cl_2 + 9 mM Et_3N, 400 MHz). Top: photoconversion of host **1** only; bottom: photoconversion of complex **1⊃3a**. In both cases, the experimental data were successfully fit to first order kinetics. b) Release and uptake cycles performed in dichloroethane with fluorescence monitoring (λ = 500 nm). hν: irradiation at 427 nm; Δ: heating at 60°C overnight.

In conclusion, a triple decker anthracene-containing foldamer capsule was designed and synthesised, which acted as a host for a T-shaped guest molecule. Photoirradiation of the host resulted in [4π + 4π] photocyclisation within the capsule backbone, lowering guest affinity and provoking its photoexpulsion. Thermal reversion of the supramolecular assembly in successive cycles was demonstrated, making this a unique example of a photo- and thermo-reversible foldaxane assembly. Further work is in progress to develop photoactivated foldaxane-based molecular machines.

Financial support from the China Scholarship Council, for a predoctoral fellowship (C.Y.) and the French National Research Agency (grant ANR-18-CE6-0018, FORESEE) is gratefully acknowledged. The work benefited from the facilities and expertise of the Biophysical and Structural Chemistry platform at IECB, CNRS UMS3033, INSERM US001, Univ. Bordeaux.

Data availability

Crystallographic data for single crystals of **1⊃3a**, which were obtained via liquid-liquid diffusion, has been deposited at the CCDC under CCDC2162063 (CIF in ESI).

a. Univ. Bordeaux, CNRS, Bordeaux INP, CBMN (UMR 5248), 2 rue Escarpit 33600 Pessac (France)

E-mail: yann.ferrand@u-bordeaux.fr

b. Current address: Department of Chemistry, School of Natural Sciences, Shiv Nadar Institution of Eminence, Greater Noida, Uttar Pradesh 201314, India.

c. Univ. Bordeaux, CNRS, Institut des Sciences Moléculaires (UMR5255), 351 cours de la Libération, 33405 Talence cedex (France)

E-mail: nathan.mcclenaghan@u-bordeaux.fr

d. Univ. Bordeaux, CNRS, INSERM, Institut Européen de Chimie Biologie (UMS3033/US001), 2 rue Escarpit 33600 Pessac (France).

e. Department of Pharmacy Ludwig-Maximilians-Universität München Butenandtstr. 5–13, 81377 Munich (Germany)

† Electronic Supplementary Information (ESI) available: See DOI: 10.1039/x0xx00000x

Notes and references

1. a) D.-W. Zhang, X. Zhao, J.-L. Hou, Z.-T. Li, *Chem. Rev.* 2012, **112**, 5271. b) G. Guichard, I. Huc, *Chem. Commun.* 2011, **47**, 5933. c) T. A. Sobiech, Y. L. Zhong; B. Gong, *Org. Biomol. Chem.* 2022, **20**, 6962. d) K. M. Kim, G. Song, S. Lee, H.-G. Jeon, W. Chae, K.-S. Jeong, *Angew. Chem. Int. Ed.* 2020, **132** 22661.
2. Y. Ferrand, I. Huc, *Acc. Chem. Res.* 2018, **51**, 970
3. a) B. Gole, B. Kauffmann, V. Maurizot, I. Huc, Y. Ferrand *Angew. Chem. Int. Ed.* 2019, **58**, 8063. b) B. Gole, B. Kauffmann, A. Tron, V. Maurizot, N. McClenaghan, I. Huc, Y. Ferrand, *J. Am. Chem. Soc.* 2022, **144**, 6894.
4. V. Koehler, A. Roy, I. Huc, Y. Ferrand, *Acc. Chem. Res.* 2022, **55**, 1074.
5. a) A. Petitjean, L. A. Cuccia, M. Schmutz, J.-M. Lehn, *J. Org. Chem.* 2008, **73**, 2481. b) T. A. Sobiech, Y. Zhong, L. S. Sanchez B., B. Kauffmann, J. K. McGrath, C. Scalzo, D. P. Miller, I. Huc, E. Zurek, Y. Ferrand, B. Gong, *Chem. Commun*. 2021, **57**, 11645. c) Y. Zhong, T.A. Sobiech, B. Kauffmann, B. Song, X. Li, Y. Ferrand, I. Huc, B. Gong, *Chem. Sci.* 2023, **14**, 4759.
6. a) R.S. Forgan, J.P. Sauvage, J.F. Stoddart, *Chem. Rev.* 2011, **111**, 5434. b) J.D. Crowley, S.M. Goldup, A.L. Lee, D.A. Leigh, R.T. McBurney, *Chem. Soc. Rev*. 2009, **38**, 1530.
7. a) Q. Gan, Y. Ferrand, C. Bao, B. Kauffmann, A. Grélard, H. Jiang, I. Huc, *Science* 2011, **331**, 1172. b) X. Wang, B. Wicher, Y. Ferrand, I. Huc, *J. Am. Chem. Soc.* 2017, **139**, 9350.
8. a) Q. Gan, X. Wang, B. Kauffmann, F. Rosu, Y. Ferrand, I. Huc, *Nat. Nanotechnol.* 2017, **12**, 447. b) S. A. Denisov, Q. Gan, X. Wang, L. Scarpantonio, Y. Ferrand, B. Kauffmann, G. Jonusauskas, I. Huc, N. D. McClenaghan, *Angew. Chem. Int. Ed.* 2016, **55**, 1328.
9. a) L. Scarpantonio, A. Tron, C. Destribats, P. Godard, N. D. McClenaghan, *Chem. Commun.* 2012, **48**, 3981. b) P. R. Ashton, V. Balzani, O. Kocian, L. Prodi, N. Spencer, J. F. Stoddart, *J. Am. Chem. Soc.* 1998, **120**, 11190.
10. A. Lamouroux, L. Sebaoun, B. Wicher, B. Kauffmann, Y. Ferrand, V. Maurizot, I. Huc *J. Am. Chem. Soc.* 2017, **139**, 14668.
11. C. Yao, B. Kauffmann, I. Huc, Y. Ferrand, *Chem. Commun*. 2022, **58**, 5789.
12. J.B. Birks, D.J. Dyson, I.H. Munro, *Proc. Roy. Soc. London A Math. & Phys. Sci.* 1963, **275** (1360), 575.
13. a) B. Daly, J. Ling, A.P. de Silva, *Chem. Soc. Rev*. 2015, **44**, 4203. b) A.P. de Silva, *J. Phys. Chem. Lett.* 2011, **2**, 2865.
14. a) A. M. Swinnen, M. Van der Auweraer, F. C. De Schryver, K. Nakatani, T. Okada and N. Mataga, *J. Am. Chem. Soc.* 1987, **109**, 321. b) A. K. Purkayastha, S. Basu, *J. Photochem.* 1979, **11**, 261.
15. M. Li, A. D. Schlüter, J. Sakamoto *J. Am. Chem. Soc.* 2012, **134**, 11721.